NANO LETTERS

Letter

pubs.acs.org/NanoLett

Symmetry Engineering of Graphene Plasmonic Crystals

Kitty Y. M. Yeung,[†] Jingyee Chee,[†] Yi Song,[‡] Jing Kong,[‡] and Donhee Ham*[,†]

[†]School of Engineering and Applied Sciences, Harvard University, Cambridge, Massachusetts 02138, United States

[‡]Electrical Engineering and Computer Science, Massachusetts Institute of Technology, Cambridge, Massachusetts 02139, United States

Supporting Information

ABSTRACT: The dispersion relation of plasmons in graphene with a periodic lattice of apertures takes a band structure. Light incident on this plasmonic crystal excites only particular plasmonic modes in select bands. The selection rule is not only frequency/wavevector matching but also symmetry matching, where the symmetry of plasmonic modes originates from the point group symmetry of the lattice. We demonstrate versatile manipulation of light-plasmon coupling behaviors by engineering the symmetry of the graphene plasmonic crystal.

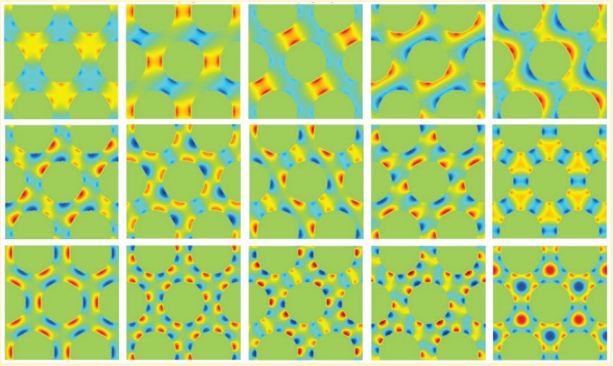

KEYWORDS: *Graphene, plasmonics, plasmonic crystals, photonic crystals, far-infrared, terahertz, point group symmetry, and bandgap engineering*

Graphene plasmons have been of significant research interest[1−11] due to their peculiar dispersion relation arising from graphene's unique electronic band structure,[10,11] sub-wavelength confinement enabled by low dimensionality,[10,12−15] and tunability.[1,10] Detailed plasmonic responses are determined by graphene geometries.[1−9] For example, scientists pioneered the field of graphene plasmonics by demonstrating localized plasmonic resonances within isolated graphene islands with the island's boundary condition setting the resonance frequency.[1−7] For another example, recent literature reported periodic structural modulations of a continuous graphene medium where delocalized plasmons interact with the periodic structure.[8,9] In particular, in ref 8 we studied a hexagonal lattice of apertures to show how the interaction of delocalized plasmons with the lattice generates bands and gaps in the plasmonic dispersion relation. This first demonstration of graphene plasmonic crystals[8] focused on proving the basic concept of the plasmonic band formation. To this end, we used far-infrared (IR) light to excite particular plasmonic modes in a select set of bands. The selection rule was not only the frequency and wavevector matching between the light and plasmonic modes but also their symmetry matching, where the symmetry of the plasmonic modes arises from the point group symmetry of the plasmonic crystals.

Significantly expanding this prior work, here we demonstrate versatile manipulation of light-plasmon coupling behaviors by engineering the point group symmetry properties of graphene plasmonic crystals. This study consists of two parts. First, to demonstrate that the symmetry-based selective light-plasmon coupling is the general feature not limited to the hexagonal lattice of our prior work, which had C_{6v} point group symmetry,[8] we fabricate graphene plasmonic crystals with square lattices of circular apertures that possess C_{4v} point group symmetry and

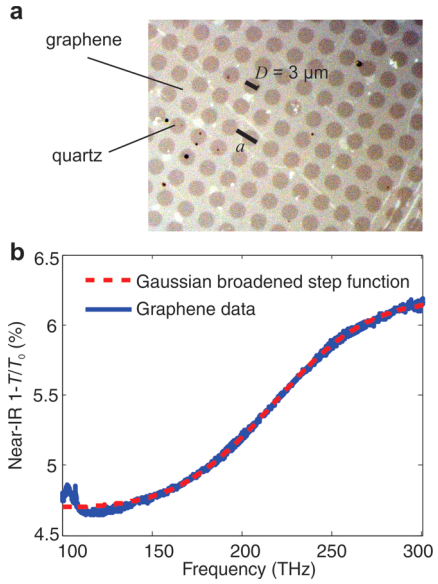

Figure 1. (a) Micrograph of a graphene plasmonic crystal with a square lattice of circular apertures (D = 3 μm; a = 4 μm). (b) Near-IR extinction spectrum (blue, solid) of the crystal in part (a) with a Gaussian-broadened-step-function fit (red, dashed).

Received: March 11, 2015
Revised: June 22, 2015
Published: July 8, 2015

DOI: 10.1021/acs.nanolett.5b00970
Nano Lett. 2015, 15, 5001−5009

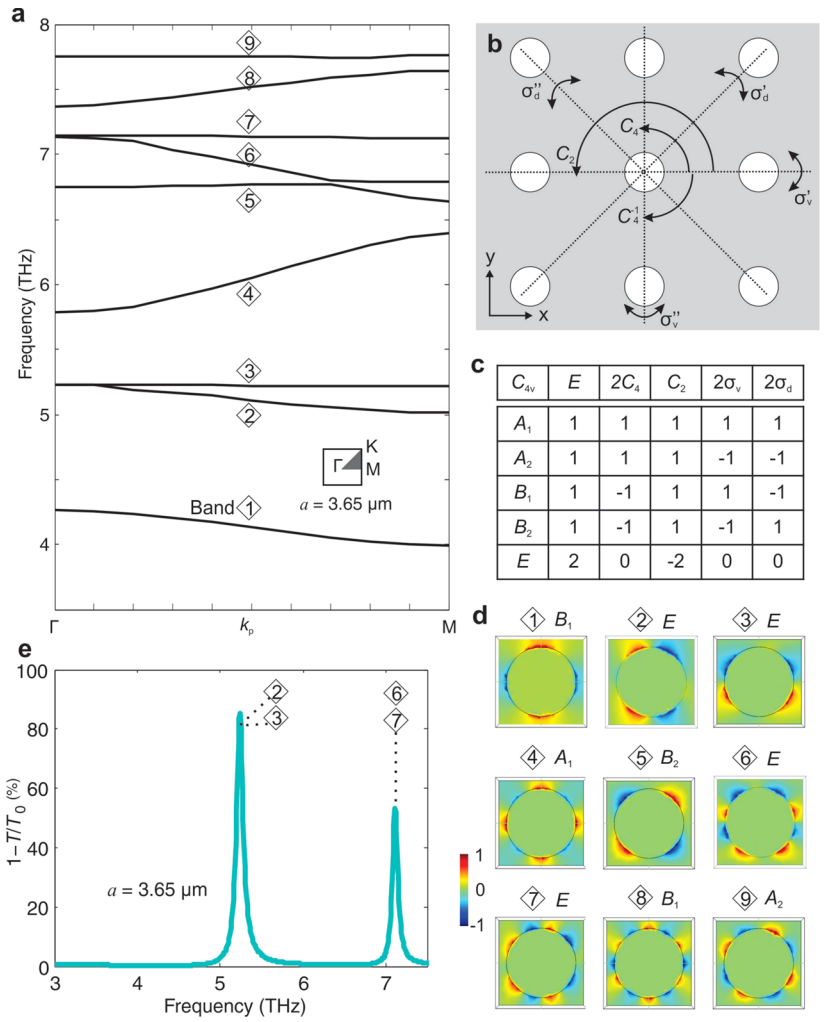

Figure 2. Simulations/theory of a square lattice of circular apertures (C_{4v} point symmetry group; D = 3 μm, a = 3.65 μm, E_F = −0.4 eV, $\tau = 5 \times 10^{-12}$ s). (a) Simulated band structure along the Γ-M direction in the square reciprocal lattice. (b,c) Elements and character table of the C_{4v} point symmetry group. (d) $E_{p,z}$ profile of each Γ-point plasmonic mode, which is labeled with the index of the band it belongs to and with the irreducible representation under the C_{4v} point symmetry group. The color bar shows normalized field strength. (e) Simulated extinction spectrum. The spectrum is independent of the polarization of the excitation plane wave light.

experimentally confirm the symmetry-based light-plasmon coupling via Fourier-transform IR spectroscopy (FTIR) in the far-IR regime. Concretely, for the square lattice of circular apertures, we identify particular plasmonic modes in select bands, whose symmetry matches the symmetry of a normally incident plane-wave far-IR light, and we then show that only these modes can be coupled to the light. These excitable modes are pairs of doubly degenerate modes with each pair excited at a single frequency, independently of the light polarization.

In the second part of this study, we demonstrate how light-plasmonic coupling behaviors are richly modified by changing the aperture shape within a given lattice. For example, as the square lattice of circular apertures with C_{4v} point group symmetry is altered to a square lattice of elliptical apertures, certain symmetries are broken and the group collapses into a C_{2v} point group. The aforementioned two-fold degeneracy of the excitable plasmonic modes is then lifted, and the resulting two nondegenerate plasmonic modes couple to normally incident plane-wave light at two separate frequencies for two orthogonal polarizations. The same line of phenomenon occurs when the aperture is altered from circle to ellipse in a hexagonal lattice. We first show these effects in simulation with a hypothetical graphene plasmonic quality factor Q in excess of 100 with which plasmonic absorption lines are sharp and the polarization-dependent absorption frequency difference most clearly manifests. We then experimentally demonstrate the effects with plasmonic crystals fabricated from chemical-vapor-deposition grown graphene samples via FTIR in the far-IR regime; while plasmonic absorption lines (FTIR extinction spectra) are broad with the plasmonic Q less than 5 in the far-IR regime, the features of the measured absorption lines still conspicuously differ for two orthogonally polarized excitation lights. Difference in their peak frequencies can also be observed. Such dependence of the light-plasmon coupling on lattice symmetry can be harnessed for applications such as far-infrared/terahertz subwavelength polarization-frequency filtering.

For the first study, we fabricate four graphene plasmonic crystals, each occupying 6 × 6 mm^2 on the same sheet of graphene. Graphene is grown on copper foil by chemical vapor deposition and transferred to a 500 μm thick single-crystal quartz substrate. All four crystals are square lattices of circular apertures. The diameter D of the circular apertures is 3 μm for all crystals. The lattice constant, a, varies from crystal to crystal: 3.65, 4, 4.5, and 5 μm (crystal with a = 4 μm is shown

DOI: 10.1021/acs.nanolett.5b00970
Nano Lett. 2015, 15, 5001−5009

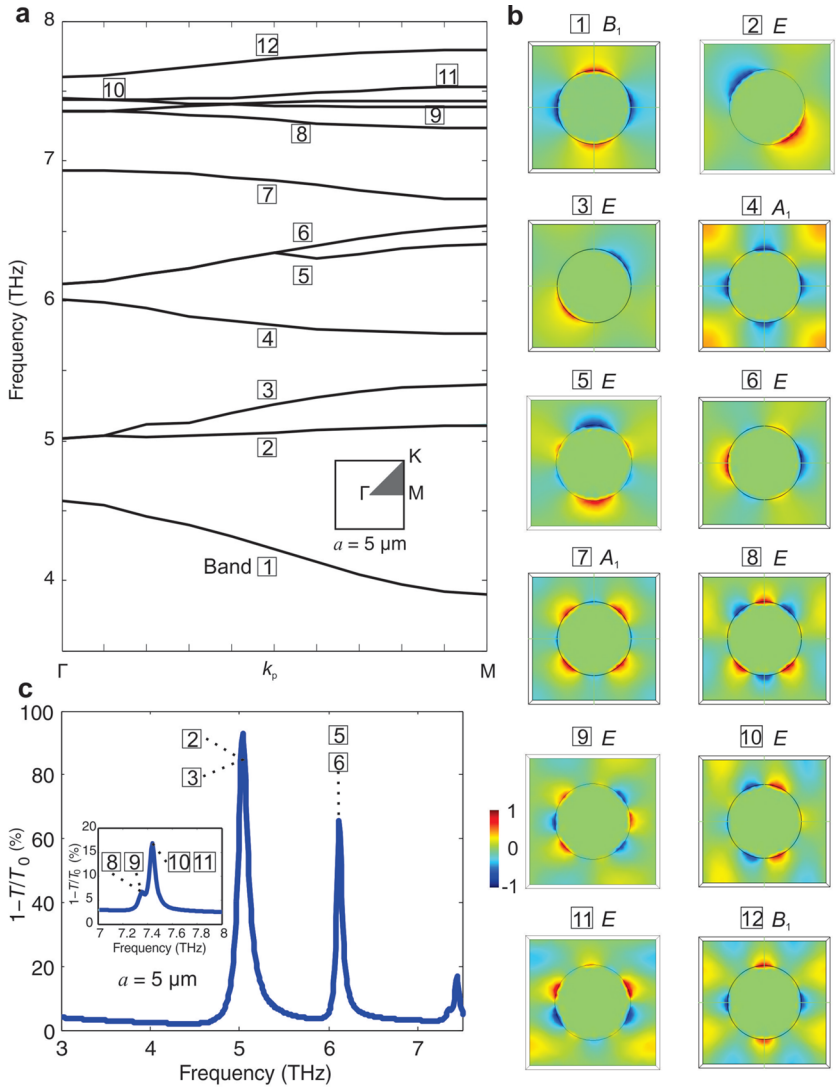

Figure 3. Simulations of a square lattice of circular apertures (C_{4v} point symmetry group; D = 3 μm, a = 5 μm, E_F = −0.457 eV, $\tau = 5 \times 10^{-12}$ s). (a) Simulated band structure along the Γ-M direction. (b) $E_{p,z}$ profile of each Γ-point plasmonic mode, labeled with band index and irreducible representation. (c) Simulated extinction spectrum (the inset is a zoom-in of the peaks in the 7−8 THz range). The spectrum is independent of the polarization of the excitation plane wave light.

in Figure 1a). Fabrication entails photolithography and O_2 plasma etching. An i-line stepper for photolithography has ∼0.65 μm resolution.

We first measure the carrier momentum relaxation time τ and Fermi level E_F as they impact plasmonic excitation line width and frequency, respectively.[8,10] To this end, we perform Hall measurements via the 4-probe Van der Pauw method in an unpatterned area (∼6 × 12 mm^2) on the same graphene sheet. $E_F \sim 0.597$ eV and $\tau \sim 6.5 \times 10^{-14}$ are the result with the latter giving a plasmonic $Q = \omega\tau$ of 2 at 5 THz. While τ may vary from crystal to crystal, as Q is low and excitation line widths are broad, we do not need to measure τ accurately for each crystal, so we use 6.5×10^{-14} s measured for the unpatterned graphene area as an estimate of τ for each crystal.

By contrast, we measure E_F for each plasmonic crystal, as the plasmonic excitation frequency depends sensitively on E_F. To this end, we measure "interband" transition via near-IR spectroscopy (this is separate from the far-IR spectroscopy, the main experiment to interrogate plasmon-light coupling, which relates to "intraband" dynamics) by using a Thermo Fisher FTIR6700 system. We measure transmission T of near-IR light through each plasmonic crystal on the quartz substrate. The reference transmission T_0 through quartz substrate not covered by graphene is also measured (this quartz substrate is transparent at frequencies below ∼8 THz and for 100−1875 THz). These lead to the extinction spectrum $1 - T/T_0$ (as the near-IR spectroscopy is performed in a N_2 atmosphere, the background transmission of N_2 is separately measured; the T and T_0 values are after calibrating out this background). We use a quartz-halogen white light lamp as the near-IR source (through an aperture with ∼4 mm diameter), a mercury cadmium telluride (MCT-A) detector, and a CaF_2 beam splitter. A mask with a pinhole (diameter ∼5 mm) is placed behind any one plasmonic crystal under test, to align the crystal to the source and detector. Near-IR light with photon energy $\hbar\omega$ in excess of $2E_F$ can induce interband transition.[11] The resulting light absorption makes the extinction spectrum a Gaussian-broadened step function (Figure 1b) with the Gaussian peak centered at $\hbar\omega = 2E_F$.[16] From this, we estimate E_F as ∼0.400, 0.417, 0.423, and 0.457 eV for the crystals with a = 3.65, 4, 4.5, and 5 μm,

DOI: 10.1021/acs.nanolett.5b00970
Nano Lett. 2015, 15, 5001−5009

respectively. Because our graphene sample is hole doped, as confirmed by the Hall measurement, the actual E_F values are negative (with the Dirac point set as the reference 0 eV).

With the measured E_F, we simulate the plasmonic band structure of the square lattice with a = 3.65 μm via finite element method (COMSOL Multiphysics).[8] Nine plasmonic bands emerge in the frequency range of 3.5−8 THz with k_p (Bloch wavenumber for plasmons) varying along the Γ-M direction in the square reciprocal lattice (Figure 2a). Normally incident far-IR light with no wavevector component on the graphene plane can couple only to plasmonic modes lying at the Γ-point (k_p = 0) of the bands. Moreover, among these Γ-point modes only a select subset, whose overlap integral with light fields does not vanish, can be excited by the light;[8] that is, symmetry between light fields and plasmonic modes must match for excitation. The plasmonic modes assume the point group symmetry of the lattice. For light and plasmonic modes to have matching symmetry, their irreducible representations under the lattice's symmetry group must be the same.

To identify the excitable plasmonic modes according to this principle, we consider first the structural symmetry of the square lattice of circular apertures. It possesses C_{4v} point group symmetry with the four-fold rotation axis, z-axis orthogonal to graphene plane, and four reflection planes (Figure 2b). Following convention, we denote the eight symmetry operations as E, $2 \times C_4$ (C_4, C_4^{-1}), C_2, $2 \times \sigma_v$ (σ_v', σ_v''), and $2 \times \sigma_d$ (σ_d', σ_d''), and the five irreducible representations as A_1, A_2, B_1, B_2, and E with the character table shown in Figure 2c.[17] Since the Γ-point plasmonic modes possess the same C_{4v} point group symmetry, each Γ-point mode can be assigned to one of the five irreducible representations. This assignment is done by examining the symmetry of the spatial profiles of $E_{p,z}$, z-component of the electric field of each Γ-point plasmonic mode at graphene surface, which is obtained during the band simulation (Figure 2d). At the same time, the normally incident plane-wave light with any linear polarization possesses symmetry with irreducible representation E (180° rotation about z-axis flips signs of the light fields) under the C_{4v} point symmetry group. Only the degenerate Γ-point modes on bands 2 and 3, and those on bands 6 and 7, are described by irreducible representation E (Figure 2d), matching the symmetry of light. Hence only these two pairs of doubly degenerate Γ-point modes are excitable, independently of light polarization.

The light's selective coupling to these particular modes is confirmed by a separate COMSOL simulation that calculates the extinction spectrum with plane-wave light excitation (Figure 2e; the spectrum is independent of the polarization of the light). The two extinction peaks obtained here occur at exactly the same frequencies of the two pairs of the degenerate Γ-point modes obtained from the band simulation. Moreover, the extinction spectrum simulation with graphene illuminated by the light also gives a profile of the electric field on the graphene plane at every frequency. This field profile corresponds to the response of graphene under the driving field of the incident plane wave. We call the z-component of this response electric field E_z in order to compare it to the $E_{p,z}$ profile of the plasmonic mode from the band simulations. The profiles of E_z that can be driven by the incident light at the extinction peaks should show the same feature as the $E_{p,z}$ profiles of the corresponding Γ-point modes with the matching symmetry to light. In fact, the doubly degenerate E_z profiles at the extinction peaks (Figure S1, Supporting Information) agree with the $E_{p,z}$ profiles of the two pairs of the degenerate Γ-point plasmonic modes (Figure 2d), showing the consistency between the band and extinction spectrum simulations.

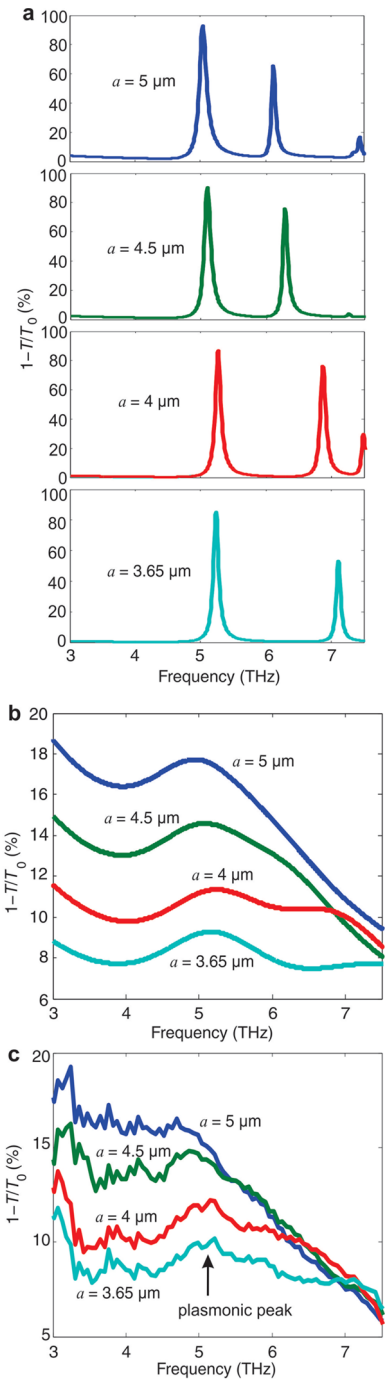

Figure 4. Measurements and simulations of four square lattices with circular apertures (C_{4v} point symmetry group; D is fixed at 3 μm across the four lattices; a varies from 5 to 4.5 to 4 to 3.65 μm). (a) Simulated extinction spectra of all four lattices ($\tau = 5 \times 10^{-12}$ s). Top and bottom panels are identical to Figures 3c and 2e, respectively. The frequency-dependent dielectric constant of quartz used in the simulations is from literature.[19] (b) Same simulations as (a) but with the measured τ of 6.5×10^{-14} s. (c) Measured Far-IR extinction spectra from FTIR experiments.

This symmetry-based light-plasmon coupling is generally applicable. For example, while the square lattice of circular apertures with a = 5 μm has a differing plasmonic band structure

DOI: 10.1021/acs.nanolett.5b00970
Nano Lett. 2015, 15, 5001−5009

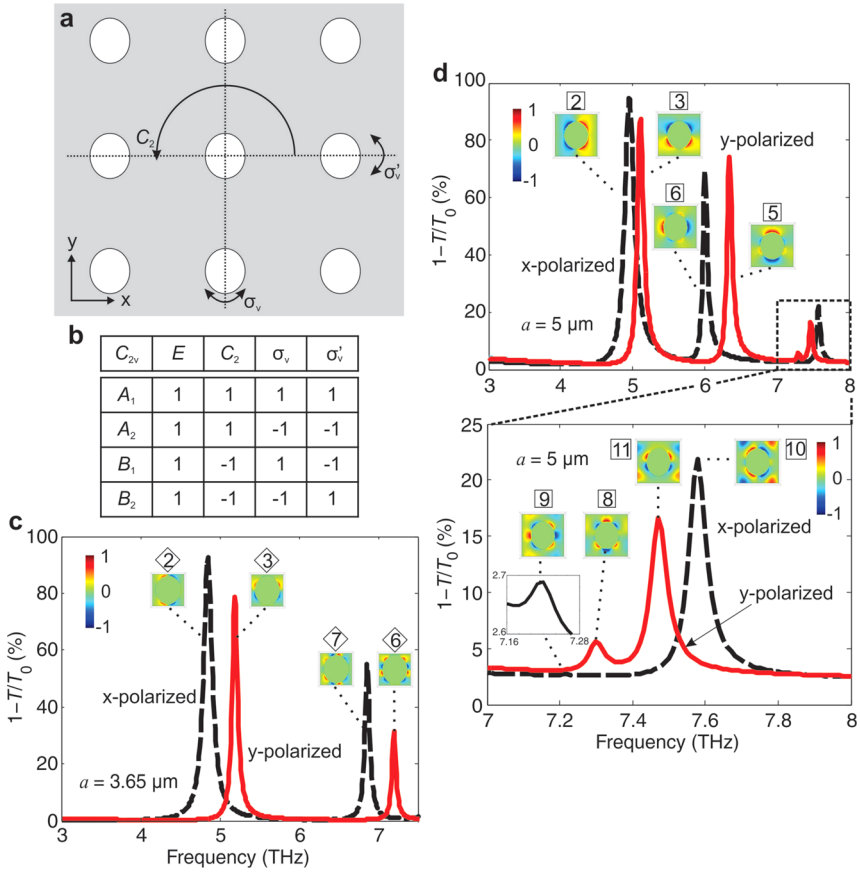

Figure 5. Simulations/theory of two square lattices with elliptical apertures (C_{2v} point symmetry group). (a,b) Elements and character table of the C_{2v} group. (c) Simulated extinction spectra of a square lattice (a = 3.65 μm) of elliptical apertures (semiminor axis = 1.5 μm, semimajor axis = 1.7 μm) with x-polarized (black, dashed) and y-polarized (red, solid) excitation light. E_F = −0.4 eV. $\tau = 5 \times 10^{-12}$. (d) The same simulation but with a = 5 μm and E_F = −0.457 eV. The bottom panel is a zoom-in of the 7−8 THz range. Both parts (c,d) show E_z profiles at the peaks; their labels are the indices of the particular bands in Figures 2 and 3 to which the original degenerate Γ-point plasmonic modes (before the degeneracy removal) belong.

(Figure 3a), again only those Γ-point modes assigned to irreducible representation E can be excited by the plane-wave light. The $E_{p,z}$ profiles of the Γ-point modes obtained from the band simulation (Figure 3b) show that four pairs of doubly degenerate Γ-point modes in bands (2, 3), (5, 6), (8, 9), and (10, 11) are assigned to the irreducible representation E. The simulated extinction peaks (Figure 3c; independent of the polarization of light) indeed occur at exactly the same frequencies as those of the four pairs of degenerate modes, confirming the symmetry-based coupling. Moreover, the four pairs of doubly degenerate E_z profiles from the extinction spectrum simulation at these four peaks (Figure S2, Supporting Information) agree with the $E_{p,z}$ profiles for the four pairs of doubly degenerate Γ-point plasmonic modes from the band simulation (Figure 3b). One apparent exception is at the lowest-frequency peak at ∼5 THz; the two degenerate E_z profiles at this peak (Figure S2, Supporting Information) seemingly differ from the two degenerate $E_{p,z}$ profiles of the degenerate Γ-point modes in bands (2, 3) at the same frequency (Figure 3b). But these two pairs of degenerate field profiles are actually equivalent, as one pair is obtained by linear superposition (addition and subtraction in this case) of the other; either pair forms a basis for the field solutions at the degenerate frequency.

Figure 4a juxtaposes simulated extinction spectra for all four square lattices of circular apertures (top and bottom panels are identical to Figures 3c and 2e), where peaks correspond to the plasmon-light coupling with matching symmetry. As a decreases, the spacing between the first and second peaks increases, because as the first Brillouin zone widens with decreasing a, fewer plasmonic bands, and thus fewer Γ-point modes, occupy a given frequency range.

All above simulated extinction spectra assumed $\tau = 5 \times 10^{-12}$ s (corresponding to plasmonic Q of ∼150 at 5 THz). While such high-quality large-area graphene is not available yet, the hypothetically sharp extinction lines were used to show the light-plasmon coupling at more than one frequency without being masked by broad lines. With the actual τ of 6.5×10^{-14} s, simulated extinction spectra are greatly broadened (Figure 4b). For a larger a, with which the lowest- and second-lowest extinction peak frequencies are closer (Figure 4a), the second peak is blurred away by the now broadened first peak (Figure 4b). For a smaller a, which separates the two peak frequencies farther (Figure 4a), both peaks become resolvable (Figure 4b).

Figure 4c shows the measured extinction spectra for all 4 plasmonic crystals, where these far-IR spectroscopy measurements are done again with the Thermo Fisher FTIR6700 system. The measurement scheme is the same as in the near-IR spectroscopy: transmission, T, of normally incident, unpolarized far-IR light through each plasmonic crystal on quartz substrate is measured, and reference transmission, T_0, through quartz substrate with no graphene on top is measured. Figure 4c is the resulting extinction, $1 - T/T_0$, for each crystal. We use an Ever-Glo IR source (beam diameter ∼8.75 mm), a polyethylene-windowed deuterated triglycine sulfate detector, and a solid

DOI: 10.1021/acs.nanolett.5b00970
Nano Lett. 2015, 15, 5001−5009

substrate beam splitter. A mask with a pinhole (diameter ~5 mm) is aligned behind any one crystal under test so that only transmission through that crystal is measured.

The measured extinction spectra of Figure 4c confirm the essence of the foregoing theory. First, when a is larger (5 and 4.5 μm), only one peak appears, but when a is reduced (4 and 3.65 μm), the spectrum shows slower roll-off because light coupling to the next excitable mode is less blurred away with decreasing a, as explained with the simulation (Figure 4b). Second, the first plasmon-light coupling peaks indeed occur around at 5 THz, as predicted by simulation. Third, the frequency of the first peak increases as a is reduced from 5 to 4.5 to 4 μm, but does not increase any more as a is further reduced to 3.65 μm, which is largely consistent with simulation (Figure 4b); in simulation, the frequency increases as a is reduced from 5 to 4.5 μm to 4 μm, just like in the measurements, and then decreases as a is further reduced to 3.65 μm. In sum, the measured extinction spectra confirm the coupling of far-IR light to particular plasmonic modes predicted by symmetry-matching considerations.

We proceed to our second focus and investigate how the light-plasmon coupling behaviors are altered when the aperture shape is modified within a given lattice. As a first demonstrational example, we change the square lattice of circular apertures with a diameter of 3 μm (as used in the experiment above) into a square lattice of elliptical apertures, where the ellipse is elongated in the y-direction with semimajor and -minor axes of 1.7 and 1.5 μm, respectively (Figure 5a). The C_{4v} point group symmetry is then reduced to the C_{2v} point group symmetry, whose character table is shown in Figure 5b. Under the C_{2v} point symmetry group, the normally incident x- and y-polarized plane-wave lights are described by distinct irreducible representations, B_2 and B_1, respectively. Thus, only Γ-point plasmonic modes whose symmetry properties are represented by B_2 or B_1 will be excited, with the former [latter] excited by x-polarized [y-polarized] light.

We verify this for a square lattice of elliptical apertures with a = 3.65 μm via extinction spectrum simulation with x- and y-polarized light. As seen in Figure 5c, E_z profiles at the two extinction peaks excited by x-polarized light have the symmetry described by B_2 irreducible representation, and E_z profiles at the other two extinction peaks excited by y-polarized light have the symmetry described by B_1 irreducible representation, as predicted. Importantly, the E_z profiles of the two polarization-dependent peaks around 5 THz [7 THz] (Figure 5c) have the same spatial features as the $E_{p,z}$ profiles of the Γ-point degenerate plasmonic modes in bands 2 and 3 [bands 6 and 7] (Figure 2d). This shows that as we alter the aperture from circle to ellipse in the square lattice, each pair of the doubly degenerate Γ-point plasmonic modes that were polarization-independently excited at a single frequency now split into the two nondegenerate Γ-point plasmonic modes, which are excited at two different frequencies and polarizations.

A similar change in the light-plasmon coupling behavior occurs as the aperture is once again altered from circle to ellipse for a square lattice with a = 5 μm (Figure 5d versus Figure 3). Each of the four peaks of Figure 3c (excitation of four pairs of doubly degenerate Γ-point plasmonic modes in bands (2, 3), (5, 6), (8, 9), and (10, 11) in the square lattice of circular apertures) now splits into two peaks (Figure 5d), one described by irreducible representation B_2 and thus excitable by x-polarized light, and the other by irreducible representation B_1 and excitable by y-polarized light. E_z profiles at the extinction peaks in this elliptical aperture case (Figure 5d) exhibit the same spatial features as $E_{p,z}$ profiles in Figure 3b in the circular aperture case; this shows once again degeneracy lifting.

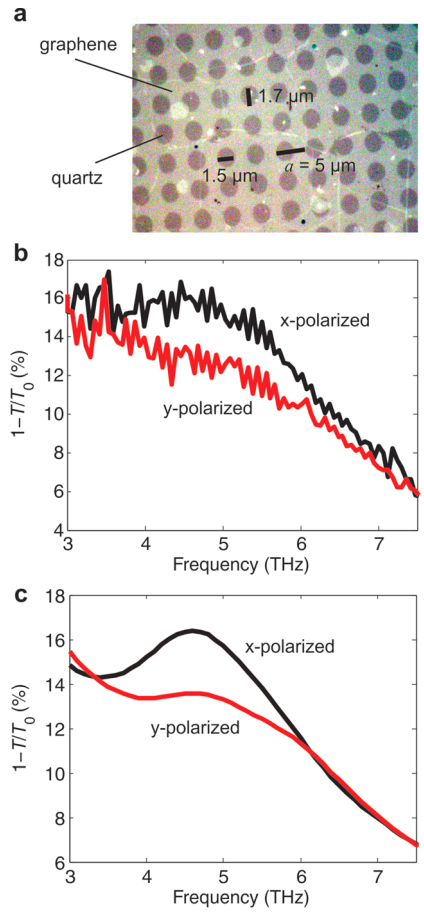

Figure 6. (a) Micrograph of a graphene plasmonic crystal with square lattice of elliptical apertures. (b) Measured extinction spectra with x-polarized (black) and y-polarized (red) excitation light. (c) Simulated extinction spectra for the two orthogonally polarized excitations, where E_F = −0.4 eV. $\tau = 6.5 \times 10^{-14}$ s are used for the simulation.

To experimentally demonstrate the polarization-dependent extinction spectra, we fabricate a square lattice of elliptical apertures on a new sheet of graphene (Figure 6a, $E_F \sim -0.400$ eV). While the foregoing simulation used a hypothetical scattering time of $\tau = 5 \times 10^{-12}$ s (plasmonic $Q > 100$) to most clearly show the polarization-dependent absorption peak frequencies with sharp absorption lines, the actual device has a plasmonic Q less than 5 and plasmonic absorption lines are broad. Nonetheless, the intrinsic absorption peak frequency dependence on polarization still causes a conspicuous difference in the measured absorption spectra features for the two orthogonally polarized excitation lights (Figure 6b). Specifically, the absorption line with x-polarized excitation light is more pronounced with a single broad peak (all other peaks are blurred out) than that with y-polarized excitation light. This is consistent with low-Q simulation with $\tau = 6.5 \times 10^{-14}$ s (Figure 6c). To affirm that this polarization dependence is due to the elliptical apertures, we conduct a control experiment with a square lattice of circular apertures fabricated on the same graphene sheet. This control experiment confirms that measured absorption spectra exhibit the same feature regardless of excitation light's polarizations (Figure S5, Supporting Information). In all of these experiments, we use Bruker Optics IF251 FIR polyethylene polarizer inserted in front of the sample.

DOI: 10.1021/acs.nanolett.5b00970
Nano Lett. 2015, 15, 5001−5009

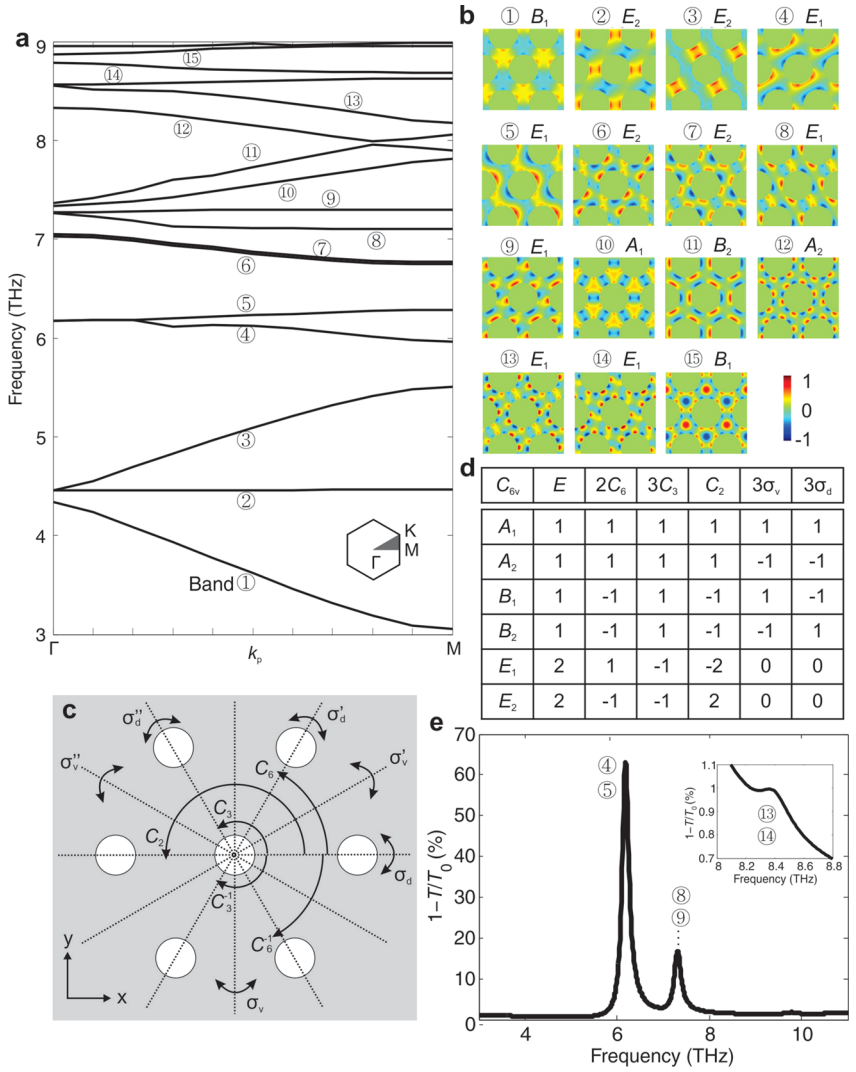

C_{6v}	E	$2C_6$	$3C_3$	C_2	$3\sigma_v$	$3\sigma_d$
A_1	1	1	1	1	1	1
A_2	1	1	1	1	-1	-1
B_1	1	-1	1	-1	1	-1
B_2	1	-1	1	-1	-1	1
E_1	2	1	-1	-2	0	0
E_2	2	-1	-1	2	0	0

Figure 7. Simulations/theory of a hexagonal lattice of circular apertures (C_{6v} point symmetry group; D = 3 μm, a = 4 μm, E_F = −0.38 eV, $\tau = 5 \times 10^{-12}$ s, SiO_2/Si substrate). (a) Simulated band structure along the Γ-M direction in the hexagonal reciprocal lattice. (b) $E_{p,z}$ profile of each Γ-point plasmonic mode. (c,d) Elements and character table of the C_{6v} point symmetry group. (e) Simulated extinction spectrum (inset is a zoom-in of the 8−8.8 THz range). The spectrum is independent of polarization of excitation plane wave light.

The same line of phenomena takes place, as we take a hexagonal lattice[8] and modify the aperture from circle (Figure 7) to ellipse (Figure 8), reducing the point group symmetry from C_{6v} to C_{2v}. Figure 7 shows the simulated band structure of the hexagonal lattice of circular apertures (D = 3 μm, a = 4 μm) with each Γ-point mode $E_{p,z}$ profile assigned to a C_{6v} irreducible representation. Its doubly degenerate Γ-point plasmonic modes (4, 5), (8, 9), or (13, 14) have symmetry described by E_1 irreducible representation under the C_{6v} point group, which is also the irreducible representation of both x- and y-polarized light under the same group.[8] Thus, only these modes can couple to light. Indeed, in the simulated extinction spectrum (Figure 7e), three peaks appear at exactly the same frequencies of the three pairs of degenerate modes (see Figure S3, Supporting Information for their E_z profiles).

When aperture changes from circle to ellipse (semiminor axis = 1.5 μm, semimajor axis = 1.7 μm along the y-direction) in the hexagonal lattice, symmetry is reduced to the C_{2v} point group (Figure 8a,b), and extinction spectra (Figure 8c,d) exhibit the impact of degeneracy removal, that is, peak splitting with polarization dependency, as compared to Figure 7e. These split peaks of Figure 8c,d are labeled with the indices of the bands in Figure 7a [(4, 5), (8, 9), and (13, 14)] that host the original degenerate modes, where we identify the original modes by comparing the $E_{p,z}$ profiles in Figure 7 and the E_z profiles at the peaks in Figure 8.

For experimental verifications of these phenomena, we fabricate a hexagonal lattice of elliptical apertures (Figure 9a, $E_F \sim -0.400$ eV, a = 4 μm, semiminor axis = 1.5 μm, semimajor axis = 1.7 μm along the y-direction). Because of the actual plasmonic Q less than 5, measured plasmonic absorption lines are broad (Figure 9b). Nevertheless, the measured absorption spectra manifest a conspicuous feature difference for the two orthogonally polarized excitation lights and the peak frequency dependence on polarization is verified. Specifically, each of the extinction spectra for x- and y-polarized excitations has a single broad peak with all other peaks masked due to the low Q, and the peak frequencies for these two spectra, estimated from the phenomenological fitting to Fano curves,[8] are ∼5.2 THz for the x-polarized excitation light and ∼5.5 THz for the y-polarized excitation light. These measurements are consistent with low-Q simulation with $\tau = 6.5 \times 10^{-14}$ s (Figure 9c). Furthermore, the

DOI: 10.1021/acs.nanolett.5b00970
Nano Lett. 2015, 15, 5001−5009

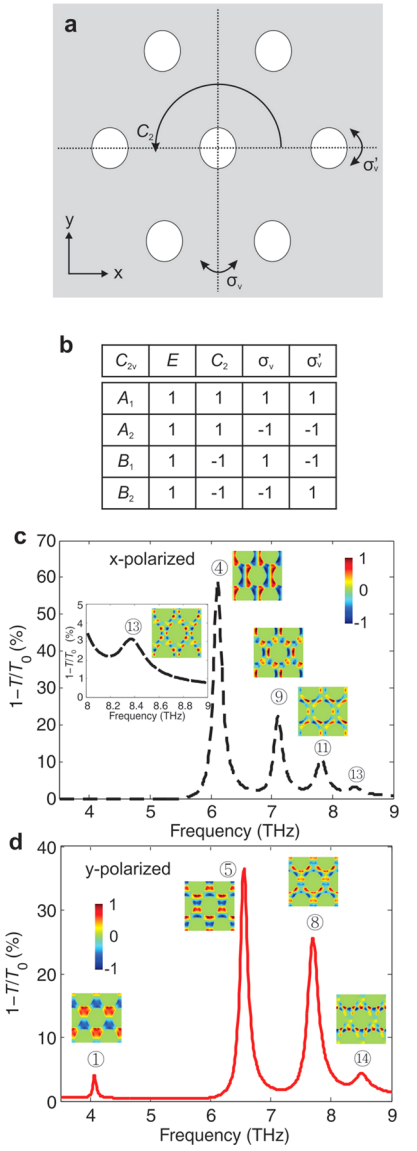

Figure 8. Simulations/theory of a hexagonal lattice of elliptical apertures (C_{2v} point symmetry group; a = 4 μm, elliptical aperture semiminor axis = 1.5 μm, semimajor axis = 1.7 μm, E_F = −0.38 eV, $\tau = 5 \times 10^{-12}$ s, SiO_2/Si substrate). (a,b) Elements and character table of the C_{2v} point symmetry group. (c,d) Simulated extinction spectra with x- and y-polarized light. The inset in part (c) shows a zoomed-in view of the 8−9 THz range. Both parts (c) and (d) show E_z profiles at the peaks, and their labels are indices of the particular bands from Figure 6a to which the original Γ-point plasmonic modes belong.

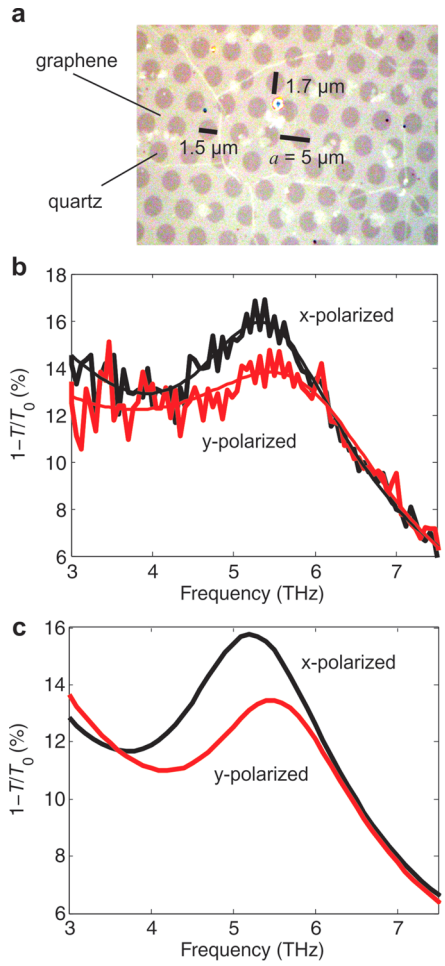

Figure 9. (a) Micrograph of a graphene plasmonic crystal with hexagonal lattice of elliptical apertures. (b) Measured extinction spectra with x-polarized (black) and y-polarized (red) excitations. (c) Simulated extinction spectra for the two orthogonally polarized excitations. E_F = −0.4 eV. $\tau = 6.5 \times 10^{-14}$ s are used for the simulation.

control experiment confirms that the extinction spectra of a hexagonal lattice with circular apertures for the two orthogonally polarized excitations exhibit no feature difference (Supporting Information, Figure S5).

Besides the degeneracy removal of already excitable modes, the aperture shape alteration can also make originally inactive plasmonic modes excitable.[17,18] The simulated extinction spectra of Figure 8c,d show this aspect of broken-symmetry as well: two additional peaks, labeled 1 and 11, are excited by light with y- and x-polarizations, respectively. These two peaks are labeled 1 and 11, as their E_z profiles (Figure 8c,d) show the same spatial features as the $E_{p,z}$ profiles of Γ-point modes in bands 1 and 11 for the hexagonal lattice with the original circular apertures (Figure 7b). These two modes, described by B_1 and B_2 irreducible representations under the C_{6v} group (under which the symmetry of light of any polarization is described by E_1 irreducible representation), were thus inactive in the hexagonal lattice of circular apertures and did not show up in Figure 7e. By contrast, in the hexagonal lattice of elliptical apertures they are described by B_1 and B_2 irreducible representations under the C_{2v} group, just as the y- and x-polarized lights are, and therefore are excited. A gradual change from circular to elliptical aperture is presented in Figure S4, Supporting Information, showing again the emergence of the active modes from the originally inactive modes. This particular effect is not resolvable in experiments, due to the low plasmonic Q.

We demonstrated symmetry-based light-plasmon coupling in graphene plasmonic crystals, and its versatile manipulation, for example, degeneracy removal, polarization dependency control, and activation switch, via alteration of the lattice symmetry. This symmetry-based plasmonic band engineering may one day lead to useful far-IR and terahertz applications, such as polarization-dependent frequency filters with subwavelength confinement.

■ ASSOCIATED CONTENT

Supporting Information

E_z profiles from extinction spectrum simulations in Figures 2e, 3c, 6e, and 7c,d. Measured extinction spectra of graphene

DOI: 10.1021/acs.nanolett.5b00970
Nano Lett. 2015, 15, 5001−5009

plasmonic crystals with square and hexagonal lattices of circular apertures; these are control experiments to be compared to Figures 6 and 9. The Supporting Information is available free of charge on the ACS Publications website at DOI: 10.1021/acs.nanolett.5b00970.

AUTHOR INFORMATION

Corresponding Author

*E-mail: donhee@seas.harvard.edu.

Notes

The authors declare no competing financial interest.

ACKNOWLEDGMENTS

D.H. acknowledges the support by the Air Force Office of Scientific Research under contract FA9550-13-1-0211 and the Office of Naval Research under contract N00014-13-1-0806. D.H. and J.K. both acknowledge the National Science Foundation STC Center for Integrated Quantum Materials under contract DMR-1231319. J.C. acknowledges financial support from National Science Scholarship, Singapore. Device fabrication was performed in part at the Center for Nanoscale Systems at Harvard University.

REFERENCES

(1) Ju, L.; Geng, B.; Horng, J.; Girit, C.; Martin, M.; Hao, Z.; Bechtel, H. A.; Liang, X.; Zettl, A.; Shen, Y. R.; Wang, F. *Nat. Nanotechnol.* **2011**, *6*, 630−634.
(2) Yan, H.; Low, T.; Zhu, W.; Wu, Y.; Freitag, M.; Li, X.; Guinea, F.; Avouris, P.; Xia, F. *Nat. Photonics* **2013**, *7*, 394−399.
(3) Brar, V. W.; Jang, M. S.; Sherrott, M.; Lopez, J. J.; Atwater, H. A. *Nano Lett.* **2013**, *13*, 2541−2547.
(4) Freitag, M.; Low, T.; Zhu, W.; Yan, H.; Xia, F.; Avouris, P. *Nat. Commun.* **2013**, *4*, 2951.
(5) Yan, H.; Xia, F.; Li, Z.; Avouris, P. *New J. Phys.* **2012**, *14*, 125001.
(6) Fang, Z.; Thongrattanasiri, S.; Schlather, A.; Liu, Z.; Ma, L.; Wang, Y.; Ajayan, P. M.; Nordlander, P.; Halas, N. J.; García de Abajo, F. J. *ACS Nano* **2013**, *7*, 2388−2395.
(7) Yan, H.; Li, X.; Chandra, B.; Tulevski, G.; Wu, Y.; Freitag, M.; Zhu, W.; Avouris, P.; Xia, F. *Nat. Nanotechnol.* **2012**, *7*, 330−334.
(8) Yeung, K. Y. M.; Chee, J.; Yoon, H.; Song, Y.; Kong, J.; Ham, D. *Nano Lett.* **2014**, *14*, 2479−2484.
(9) Zhu, X.; Wang, W.; Yan, W.; Larsen, M. B.; Bøggild, P.; Pedersen, T. G.; Xiao, S.; Zi, J.; Mortensen, N. A. *Nano Lett.* **2014**, *14*, 2907.
(10) Yoon, H.; Forsythe, C.; Wang, L.; Tombros, N.; Watanabe, K.; Taniguchi, T.; Hone, J.; Kim, P.; Ham, D. *Nat. Nanotechnol.* **2014**, *9*, 594.
(11) Das Sarma, S.; Adam, S.; Hwang, E. H.; Rossi, E. *Rev. Mod. Phys.* **2011**, *83*, 407−470.
(12) Yoon, H.; Yeung, K. Y. M.; Umansky, V.; Ham, D. *Nature* **2012**, *488*, 65−69.
(13) Yeung, K. Y. M.; Yoon, H.; Andress, W.; West, K.; Pfeiffer, L.; Ham, D. *Appl. Phys. Lett.* **2013**, *102*, 021104.
(14) Andress, W.; Yoon, H.; Yeung, K. Y. M.; Qin, L.; West, K.; Pfeiffer, L.; Ham, D. *Nano Lett.* **2012**, *12*, 2272−2277.
(15) Yoon, H.; Yeung, K. Y. M.; Kim, P.; Ham, D. *Philos. Trans. R. Soc., A* **2014**, *372*, 20130104.
(16) Yan, H.; Xia, F.; Zhu, W.; Freitag, M.; Dimitrakopoulos, C.; Bol, A. A.; Tulevski, G.; Avouris, P. *ACS Nano* **2011**, *5*, 9854−9860.
(17) Sakoda, K. *Optical Properties of Photonic Crystals*, 2nd ed.; Springer: Berlin, 2005.
(18) Kilic, O.; Digonnet, M.; Kino, G.; Solgaard, O. *Opt. Express* **2008**, *16*, 13090−13103.
(19) Palik, E. D. *Handbook of Optical Constants of Solids*; Academic Press: New York, 1985.

DOI: 10.1021/acs.nanolett.5b00970
Nano Lett. 2015, 15, 5001−5009